

Reliable approach for bistatic scattering of three-dimensional targets from underlying rough surface based on parabolic equation

Dong-Min Zhang(张东民), Cheng Liao(廖成), Liang Zhou(周亮), Xiao-Chuan Deng(邓小川), Ju Feng(冯菊)

Citation: Chin. Phys. B . 2018, 27(7): 074102. **doi:** 10.1088/1674-1056/27/7/074102

Journal homepage: http://cpb.iphy.ac.cn; http://iopscience.iop.org/cpb

What follows is a list of articles you may be interested in

Influence of cutting off position of plasma filament formed by two-color femtosecond laser on terahertz generation

Zhan-Qiang Xue(薛占强), Li-Ping Shang(尚丽平), Hu Deng(邓琥), Qian-Cheng Zhang(张前成), Quan-Cheng Liu(刘泉澄), Wei-Wei Qu(屈薇薇), Zhan-Feng Li(李占锋), Shun-Li Wang(王顺利)

Chin. Phys. B . 2018, 27(5): 054101. **doi:** 10.1088/1674-1056/27/5/054101

Confinement of Bloch surface waves in a graphene-based one-dimensional photonic crystal and sensing applications

Xiu-Juan Zou(邹秀娟), Gai-Ge Zheng(郑改革), Yun-Yun Chen(陈云云)

Chin. Phys. B . 2018, 27(5): 054102. **doi:** 10.1088/1674-1056/27/5/054102

Electromagnetic backscattering from one-dimensional drifting fractal sea surface II:Electromagnetic backscattering model

Tao Xie(谢涛), William Perrie, Shang-Zhuo Zhao(赵尚卓), He Fang(方贺), Wen-Jin Yu(于文金), Yi-Jun He(何宜军)

Chin. Phys. B . 2016, 25(7): 074102. **doi:** 10.1088/1674-1056/25/7/074102

An iterative analytic-numerical method for scattering from a target buried beneath a rough surface

Xu Run-Wen, Guo Li-Xin, Wang Rui

Chin. Phys. B . 2014, 23(11): 114101. **doi:** 10.1088/1674-1056/23/11/114101

Bidirectional reflectance distribution function modeling of one-dimensional rough surface in the microwave band

Guo Li-Xin, Gou Xue-Yin, Zhang Lian-Bo

Chin. Phys. B . 2014, 23(11): 114102. **doi:** 10.1088/1674-1056/23/11/114102

Reliable approach for bistatic scattering of three-dimensional targets from underlying rough surface based on parabolic equation*

Dong-Min Zhang(张东民)[1,2], Cheng Liao(廖成)[1,†], Liang Zhou(周亮)[1], Xiao-Chuan Deng(邓小川)[1], and Ju Feng(冯菊)[1]

[1] *Institute of Electromagnetics, Southwest Jiaotong University, Chengdu* 610031, *China*
[2] *Science and Technology on Electronic Information Control Laboratory, Chengdu* 610031, *China*

(Received 18 September 2017; revised manuscript received 7 March 2018; published online 25 June 2018)

A parabolic equation (PE) based method for analyzing composite scattering under an electromagnetic wave incidence at low grazing angle, which composes of three-dimensional (3-D) electrically large targets and rough surface, is presented and discussed. A superior high-order PE version is used to improve the accuracy at wider paraxial angles, and along with the alternating direction implicit (ADI) differential technique, the computational efficiency is further improved. The formula of bistatic normalized radar cross section is derived by definition and near-far field transformation. Numerical examples are given to show the validity and accuracy of the proposed approach, in which the results are compared with those of Kirchhoff approximation (KA) and moment of method (MoM). Furthermore, the bistatic scattering properties of composite model in which the 3-D PEC targets on or above the two-dimensional Gaussian rough surfaces under the tapered wave incidence are analyzed.

Keywords: parabolic equation, rough surface, alternating direction implicit (ADI) difference, normalized radar cross section

PACS: 41.20.Jb, 41.20.–q, 42.25.Bs **DOI:** 10.1088/1674-1056/27/7/074102

1. Introduction

Analysis of electromagnetic scattering from targets and underlying randomly rough surface has important value in radar detection and identification, environment monitoring, and remote sensing.[1–8] As a result of the complex interactions between the targets and the randomly rough surface, the scattering characteristics are significantly different from those in free space, such as the ships on the sea, the low flying aircrafts, and missiles. In dealing with such coupling models, some pure numerical methods have been designedly used due to their significant advantages in accuracy and versatility, such as the integral equation approach (IE),[2,3] finite element method (FEM),[4] and finite difference time domain method (FDTD).[5,6] However, the huge number of unknowns will consume intolerable amount of computing resources and computing time for the three-dimensional (3-D) case, especially at low grazing angle incidence.

The PE is derived from the Helmholtz equation by separating the forward and backward propagation term, which was first proposed by Leontovich and Fock to study the electromagnetic wave propagation on the earth's surface in 1946.[9] As an efficient marching algorithm which requires only a small amount of computing resources and computation time, PE has been widely applied to solve the large-scale electromagnetic scattering problems recently.[10–16] Besides, the numerical results show that the 3-D targets ranging in size from a wavelength to several hundred are available for this algorithm. However, most of the previous works have focused on the isolated volumetric objects in free space.

In this paper, PE is developed to solve the bistatic scattering of 3-D electrically large targets from underlying rough surfaces. For constructing the composite scattering model, the method of Monte Carlo simulation is applied to simulate the rough sea surfaces with sea spectrum functions.[17] Considering the paraxial limitation caused by the pseudo differential operator,[12] the validated angle of the traditional PE is so narrow that it is not applicable for the composite scattering problems. Consequently, a superior PE version is used for improving the computational accuracy at wider paraxial angles by highorder polynomial approximation. Besides, by introducing the alternating direction implicit (ADI) technology, the highorder matrix inversion in traditional difference method is avoided, which significantly improves the computational efficiency. Moreover, the normalized radar cross sections (NRCS) under the tapered wave incidence at low grazing angles are obtained by the near-far field transformation. To illustrate the correctness and performance of the algorithm, the scattering coefficients of rough sea surfaces are calculated to compare with both Kirchhoff approximation (KA) method and moment of method (MoM), and the result of composite scattering from a PEC target above the finite plane ground is verified by commercial software using a solver of the multilevel fast multipole accelerated MoM (MLFMM). In addition, the compos-

*Project supported by the National Natural Science Foundation of China (Grant No. 61771407).
†Corresponding author. E-mail: c.liao@swjtu.edu.cn
© 2018 Chinese Physical Society and IOP Publishing Ltd

ite scattering examples of a 3-D PEC target on and above the two-dimensional (2-D) Gaussian rough surfaces under the tapered wave incidence at low grazing angle are analyzed and discussed.

This paper is organized as follows. The high-order parabolic equation with the introduced ADI difference technique is depicted concretely in Section 2. The formula of bistatic NRCS under the tapered wave incidence is given in Section 3. Several numerical tests are given to illustrate the correctness and performance of the algorithm, and examples of 3-D composite scattering are discussed in Section 4. The conclusions are presented in Section 5.

2. High-order PE with efficient ADI technique

In Cartesian coordinates, the time-dependence of the field is assumed to be $\mathrm{e}^{-\mathrm{i}\omega t}$, and the electromagnetic fields component $\psi(x,y,z)$ satisfies the wave equation. By introducing a reduced function $u(x,y,z) = \mathrm{e}^{-\mathrm{i}k_0 x}\psi(x,y,z)$, and splitting the wave equation into a forward and a backward propagation term, the parabolic equation which reflects the propagation of electromagnetic waves along the x direction can be obtained

$$\frac{\partial u(x,y,z)}{\partial x} = -\mathrm{i}k_0(1-\sqrt{1+Q}), \tag{1}$$

where Q is defined as

$$Q = \frac{1}{k_0^2}\left(\frac{\partial^2}{\partial y^2}+\frac{\partial^2}{\partial z^2}\right)+n^2(x,z)-1. \tag{2}$$

For electromagnetic scattering problems, the refractive index n can be regarded as unity. The solution for differential equation (1) can be expressed as

$$u(x+\Delta x,y,z) = \mathrm{e}^{\mathrm{i}k_0\Delta x\left(\sqrt{1+Q}-1\right)}u(x,y,z). \tag{3}$$

As the pseudo differential operator $\sqrt{1+Q}$ is difficult to solve numerically, some approximation is made to rationalize the operator. In traditional PE which uses the first-order Taylor expansion, the maximum paraxial angle that can be accurately calculated is only 15° to 20°.[11] In order to obtain a superwide angle solution, in this paper, a high-order rational polynomial is used to approximate the exponential terms,[19] which makes the maximum validated angle approach 70° with the order of polynomial $L=8$

$$\mathrm{e}^{\mathrm{i}k_0\Delta x\left(\sqrt{1+Q}-1\right)} \sim 1+\sum_{l=1}^{L}\frac{a_l Q}{1+b_l Q}. \tag{4}$$

Substitute Eq. (4) into Eq. (3), the high-order PE can be written as

$$u(x+\Delta x,y,z) = \sum_{l=1}^{L} w_l(x+\Delta x,y,z), \tag{5}$$

$$w_l(x+\Delta x,y,z) = \frac{1+(La_l+b_l)Q}{L+Lb_lQ}u(x,y,z), \tag{6}$$

where the complex coefficients a_l and b_l can be obtained by Newton method.[20] The field on $x+\Delta x$ can be obtained from the marching plane at x using an iterative approach. As the PE itself reflects the diffraction effect of the electromagnetic wave, the discrete rough surfaces can be easily integrated into the algorithm using the relevant boundary conditions.[15]

In order to discrete the PE, the finite difference method of Crank–Niclson (CNFD) type is usually used for 2-D applications, but it's not a wise choice for 3-D case because of the huge amount of computation from the high-order matrix inversions. The ADI difference method reduces the computational cost significantly by decomposing the transversal planes line by line and using the explicit and implicit difference scheme alternately.[18] The ADI difference scheme for high-order PE can be derived from the CNFD method directly. The derivation of the formula is given below.

For Eq. (6), we use the central difference to discrete the second-order differential, and the scheme can be written as

$$\begin{aligned}&\left(1+\frac{b_l}{k^2\Delta y^2}\sigma_y+\frac{b_l}{k^2\Delta z^2}\sigma_z\right)Lw_{li,j}^{m+1}\\ &=\left(1+\frac{La_l+b_l}{k^2\Delta y^2}\sigma_y+\frac{La_l+b_l}{k^2\Delta z^2}\sigma_z\right)u_{i,j}^{m},\end{aligned} \tag{7}$$

where

$$\begin{aligned}\sigma_y w_{li,j}^{m+1} &= w_{li+1,j}^{m+1}-2w_{li,j}^{m+1}+w_{li-1,j}^{m+1},\\ \sigma_z w_{li,j}^{m+1} &= w_{li,j+1}^{m+1}-2w_{li,j}^{m+1}+w_{li,j-1}^{m+1}.\end{aligned} \tag{8}$$

By adding a fixed term to both sides of the equation (7)

$$\begin{aligned}&\left(1+\frac{b_l\sigma_y}{k^2\Delta y^2}+\frac{b_l\sigma_z}{k^2\Delta z^2}+\frac{b_l^2\sigma_y\sigma_z}{\left(k^2\Delta y^2\right)\left(k^2\Delta z^2\right)z}\right)Lw_{li,j}^{m+1}\\ &=\left(1+\frac{(La_l+b_l)\sigma_y}{k^2\Delta y^2}+\frac{(La_l+b_l)\sigma_z}{k^2\Delta z^2}+\frac{(La_l+b_l)^2\sigma_y\sigma_z}{\left(k^2\Delta y^2\right)\left(k^2\Delta z^2\right)}\right)u_{i,j}^{m},\end{aligned} \tag{9}$$

Eq. (9) can be rewritten as

$$\begin{aligned}&\left(1+\frac{b_l}{k^2\Delta y^2}\sigma_y\right)\left(1+\frac{b_l}{k^2\Delta z^2}\sigma_z\right)Lw_{li,j}^{m+1}\\ &=\left(1+\frac{La_l+b_l}{k^2\Delta y^2}\sigma_y\right)\left(1+\frac{La_l+b_l}{k^2\Delta z^2}\sigma_z\right)u_{i,j}^{m}.\end{aligned} \tag{10}$$

Then, we introduce a virtual intermediate marching plane $x=\left(m+\frac{1}{2}\right)\Delta x$, and split Eq. (10) into two mutually independent directions, then the ADI difference scheme for high-order PE can be obtained

$$\begin{cases}\left(1+\dfrac{b_l\sigma_y}{k^2\Delta y^2}\right)Lw_{li,j}^{m+\frac{1}{2}}=\left(1+\dfrac{(La_l+b_l)\sigma_z}{k^2\Delta z^2}\right)u_{i,j}^{m},\\ \left(1+\dfrac{b_l\sigma_z}{k^2\Delta z^2}\right)Lw_{li,j}^{m+1}=\left(1+\dfrac{(La_l+b_l)\sigma_y}{k^2\Delta y^2}\right)u_{i,j}^{m+\frac{1}{2}}.\end{cases} \tag{11}$$

Note that Eq. (5) can be solved in an iterative manner. By using the ADI difference technique, the 3-D problem is converted into a series of 2-D problems. The scattered field in the entire computational region can be obtained with given initial field and suitable boundary conditions. The marching strategy for ADI high-order PE method is shown in Fig. 1.

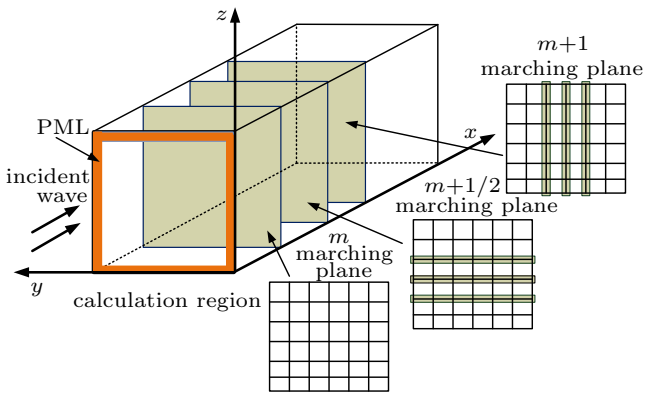


Fig. 1. (color online) The marching strategy for ADI high-order PE.

3. Bistatic NRCS formulation

A sketch map of the composite scattering model is shown in Fig. 2. In order to eliminate the truncation errors caused by rough surfaces, the plane wave is generally replaced by tapered incident wave in the electromagnetic scattering calculation, and the famous Thorsos tapered incident wave is used in this paper. The expression in 3-D coordinates is

$$u_i(x,y,z) = \exp[jk_0(x\sin\theta_i\cos\varphi_i + y\sin\theta_i\sin\varphi_i - z\cos\varphi)(1+w)] \times \exp(-(t_x+t_y)), \tag{12}$$

$$\begin{cases} t_x = \dfrac{(x\cos\theta_i\cos\varphi_i + y\cos\theta_i\sin\varphi_i + z\sin\theta_i)^2}{g^2\cos^2\theta_i}, \\ t_y = \dfrac{(-x\sin\varphi_i + y\cos\varphi_i)^2}{g^2}, \\ w = \dfrac{1}{k_0^2}\left[\dfrac{2t_x-1}{g^2\cos^2\theta_i} + \dfrac{2t_y-1}{g^2}\right], \end{cases} \tag{13}$$

where k_0 is the wavenumber in free space. The tapering width parameter g needs to satisfy the requirements of wave equation, correlation length, and energy truncation. Besides, it is related to the target size and the incident angle θ_i, which was discussed in detail in Ref. [21].

NRCS is usually used to evaluate the average scattering characteristics of distributed targets, which is defined as

$$\sigma = \lim_{r\to\infty} 4\pi r^2 \frac{|E_s|^2}{|E_i|^2}, \tag{14}$$

where r is the position vector; E_i and E_s are the incident and scattered fields, respectively. Through near-far field transformation, the bistatic NRCS in direction (θ_s, φ_s) under the tapered wave incidence can be expressed as

$$\sigma(\theta_s,\varphi_s) = \frac{k^2\sin^2\theta_s}{\pi P_i} \times \left| \iint (E_s(x_0,y,z)) \cdot \mathrm{e}^{-\mathrm{i}k_0\cos\theta_s(y\cos\varphi_s + z\sin\varphi_s)}\,\mathrm{d}y\mathrm{d}z \right|^2, \tag{15}$$

where the incident power of the tapered wave is

$$P_i = \frac{\pi}{2}g^2\cos\theta_i \cdot \left[1 - \frac{1+\cos^2\theta_i + 2\tan^2\theta_i}{2(k_0 g\cos\theta_i)^2}\right]. \tag{16}$$

Note that the scattered field $E_s(x_0,y,z)$ can directly be obtained in the transverse plane of the PE model located beyond the object.

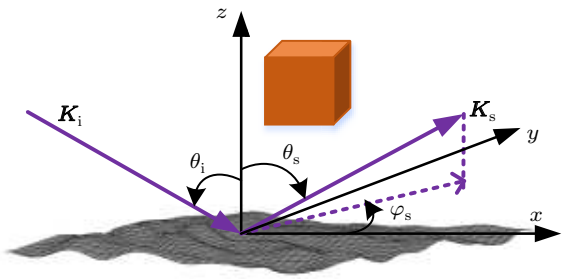


Fig. 2. (color online) The composite model of target and rough surface.

4. Results and discussion

In this section, the calculation model for composite scattering based on PE is discussed and analyzed by some numerical tests. In this paper, the rough surfaces and targets are regarded as PEC objects and the discrete sizes $(\mathrm{d}x, \mathrm{d}y, \mathrm{d}z)$ are set to $\lambda/10$, where λ is the wavelength of the electromagnetic wave. The electromagnetic wave is horizontally polarized. All calculations are performed on a six-core workstation with 16 GB memory, and the configured processor is Intel(R) Xeon(R) CPU E5-2620v3 with a dominant frequency of 2.4 GHz. The complex coefficients for the polynomial approximations in high-order PE are given in Table 1.

Table 1. The complex coefficients for the polynomial approximation in high-order PE ($L = 8$, $\mathrm{d}x = 0.1\lambda$).

l	a_l	b_l
1	(−0.072273, 0.060041)	(0.041224, −0.040126)
2	(0.006644, 0.010787)	(0.879288, −0.007309)
3	(−0.016274, −0.003111)	(−0.005525, −0.013040)
4	(0.023252, 0.040694)	(0.507202, −0.025459)
5	(0.001717, 0.002761)	(0.993461, −0.001894)
6	(0.011166, 0.113655)	(0.141675, −0.047087)
7	(0.014151, 0.023484)	(0.708478, −0.015508)
8	(0.031616, 0.065848)	(0.306731, −0.036240)

4.1. Verification and discussion

In order to show the correctness of the PE model for electromagnetic scattering from rough surfaces, and also, to show the algorithm performance, we first calculate the one-dimensional (1-D) rough surface with no target, i.e., neglecting the transverse diffraction of electromagnetic waves. The results of scattering coefficient are compared with those of KA method and MoM which are widely used in the computation of electromagnetic scattering from the rough sea surface.

In this numerical example, the frequency of Thorsos tapered wave with an incident angle of 75° is set to 1 GHz, and

the tapering width parameter $g = 50\lambda$. The observed scattering angle is set to $\theta_s \in [30°, 90°]$, $\varphi_s = 0°$. The discrete size of the computational region for PE model is $N_x \times N_z = 2048 \times 2000$. The rough sea surfaces are simulated by Monte Carlo realization with the famous Pierson–Morkowitz (P–M) spectrum.[17]

The simulation results under different wind speeds obtained via PE model are given in Figs. 3 and 4, which show that the MoM, KA method, and PE method are in agreement with each other. As the results of MoM are usually considered to be the most reliable for the high precision of the algorithm, we can regard it as a reference solution. As can be seen, PE method shows smaller errors than KA method. Note that the latter is a high frequency approximation method which neglects multiple reflections and diffractions of the electromagnetic waves. In Fig. 3, the mean error for KA method relative to MoM is 4.52 dB, and 1.97 dB for PE method. In Fig. 4, the mean error for KA method is 3.76 dB, also larger than that of PE method, which is only 1.89 dB. In addition, to illustrate the performance of the PE algorithms, the computational memory and CPU running time for algorithm program are compared with those of KA method and MoM, as shown in Table 2. Results show that the memory consumption and CPU computing time for PE method are slightly larger than those of KA method, but much less than those of MoM.

Table 2. Comparison of memory and CPU time requirement among different methods.

	CPU time	Memory
KA	2.66 s	76.0 MB
PE	8.43 s	77.9 MB
MoM	183.65 s	139.9 MB

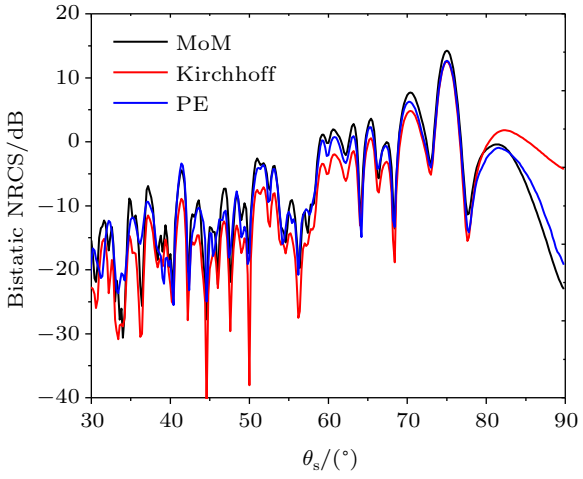


Fig. 3. (color online) NRCS of the rough sea surface under a wind speed of 4 m/s.

The following examples are extended to the 3-D calculation case, which involves far more unknowns. Figure 5 shows the simulation results of 2-D Gaussian rough surface obtained from PE and KA method, where the correlation lengths of the simulated rough surface in both x- and y-direction are set to 0.5 m, and the root-mean-square (RMS) height is 0.15 m. The incident angle is fixed at $\theta_i = 70°$, $\varphi_s = 0°$, and the observed scattering angle is set to $\theta_s \in [25°, 90°]$, $\varphi_s = 0°$. As shown, the two curves coincide with each other.

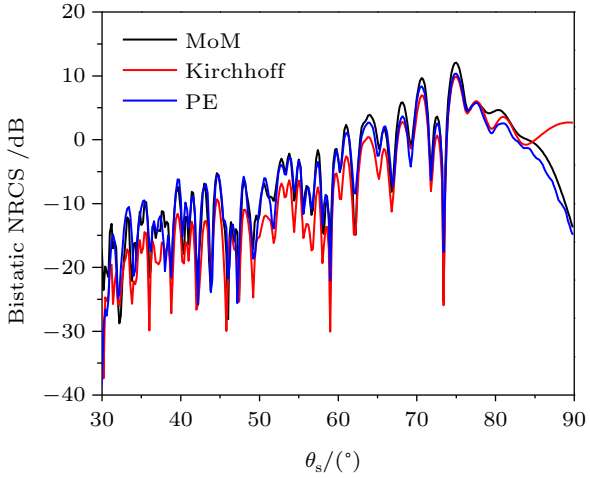


Fig. 4. (color online) NRCS of the rough sea surface under a wind speed of 10 m/s.

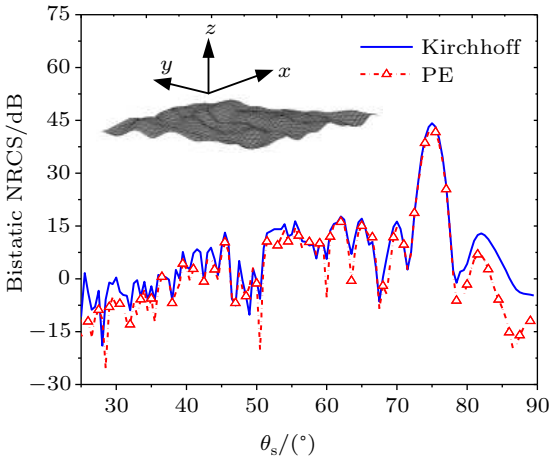


Fig. 5. (color online) NRCS of 2-D rough surface with Gaussian spectrum.

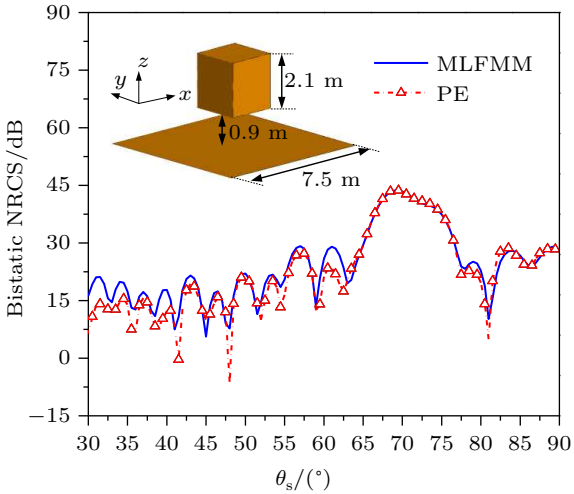


Fig. 6. (color online) NRCS of a PEC cube and underlying finite flat ground compared with MLFMM.

In order to verify the correctness of the coupling field, PE is used to calculate the coupling scattering from a PEC cube target and underlying PEC finite flat ground. The result is compared with that of the commercial software using a MLFMM solver. In this example, a plane wave of unit amplitude with a frequency of 1 GHz is used. The incident angle is fixed at $\theta_i = 70°$, $\varphi_s = 0°$, and the observed scattering angle is set to $\theta_s \in [30°, 90°]$, $\varphi_s = 0°$. The dimension of flat ground is 7.5 m×7.5 m. The PEC cube with a side length of 2.1 m is placed above the flat ground, and the distance between them is 0.9 m, as depicted in Fig. 6. The two curves coincide with each other, which also proves the correctness of the method.

4.2. Bistatic composite scattering examples

In this section, combined with numerical examples, the composite scattering characteristic of a 3-D PEC target and underlying rough sea surface under the tapered wave incidence at low grazing angle are discussed.

Unlike free space, for an object located above rough surface, multiple reflections of electromagnetic wave usually occur between the target and the underlying rough surface, and part of which are greater than the angle of 15° from the paraxial direction. Consequently, the high-order PE introduced in this paper with an available angle up to 70° is more suitable for such composite scattering models compared with the traditional narrowangle version. Figure 7 shows the bistatic NRCS of a missile-like target above the rough sea surface using ADI high-order PE method. The length and radius of the missile-like target is 5.8 m and 0.62 m, respectively, and the vertical distance between the missile and sea level is set to 1.8 m. The correlation lengths and RMS height of the 2-D Gaussian random rough sea surface are set to 0.5 m and 0.15 m, respectively. The frequency of Thorsos tapered incident wave is 1 GHz. The incident angle is fixed at $\theta_i = 70°$, $\varphi_s = 0°$, and the observed scattering angles are set to $\theta_s \in [30°, 90°]$, $\varphi_s = 0°$. The two curves represent the result of target underlying rough surface and target in free space. As seen in Fig. 7, the scattering characteristic of the composite model greatly differs from that of the isolated target in free space. As the contribution for the total scattering field comes from the target, rough sea surface, and their coupling interaction, the composite model shows greater values overall. Besides, both have the maximum values in the mirror direction.

As a result of the interaction between the rough surface and the target, different sea surface roughness will have significant influence on bistatic NRCS of the composite model. The computed results for different correlation lengths and RMS heights of the Gaussian rough surface are given to illustrate this influence while other parameters remain the same, as described in Fig. 8. In this example, when the sea surface's correlation length and RMS height are 1 m and 0.25 m, respectively, which has the largest surface roughness, the coherent scattering component becomes smaller and the incoherent scattering component increases. As a result, the maximum peak value in the mirror direction decreases, while the amplitude from the mirror direction increases markedly. Figure 9 gives the numerical results of the coupling model under different incident angles, which indicates that the bistatic NRCS is also related with the incident angle of electromagnetic wave, and the ADI high-order PE method can also be used to simulate the influence effectively.

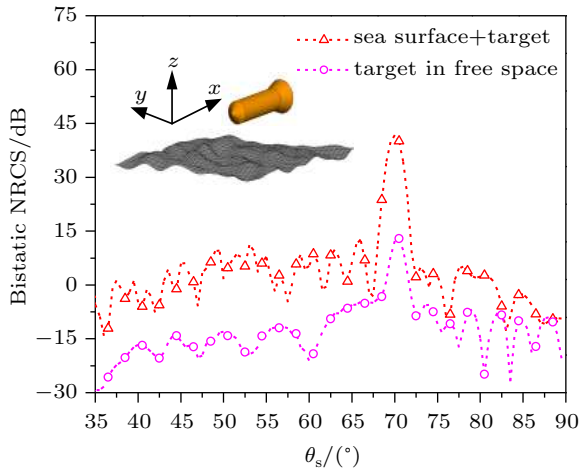


Fig. 7. (color online) Bistatic scattering from a missile-like target above Gaussian sea surface.

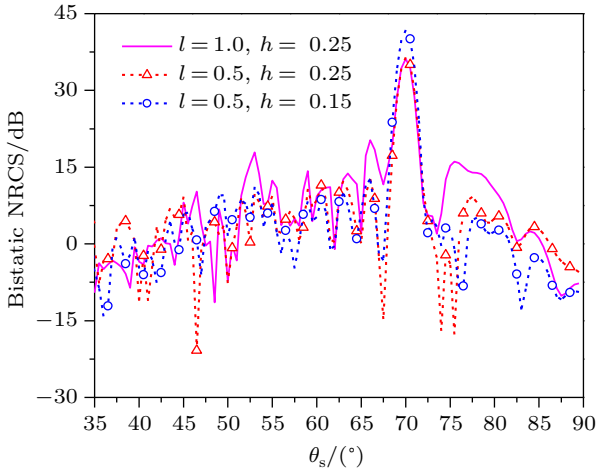


Fig. 8. (color online) Bistatic scattering of a missile-like target above the sea surface with different correlation lengths and RMS heights.

In Fig. 10, another numerical example is given where a ship-like target with the size of 12.6 m × 3.2 m × 2.4 m on the 2-D Gaussian rough sea surface. The correlation lengths and RMS height of the 2-D Gaussian rough surface are set to 1 m and 0.25 m, respectively. The frequency of Thorsos tapered incident wave is 300 MHz and the incident angle is fixed at $\theta_i = 70°$, $\varphi_s = 0°$. The observed scattering angles are set to $\theta_s \in [30°, 90°]$, $\varphi_s = 0°$. The bistatic NRCS of the target underlying rough surface and the target in free space are shown

in different curves and a similar conclusion can be obtained from the former example.

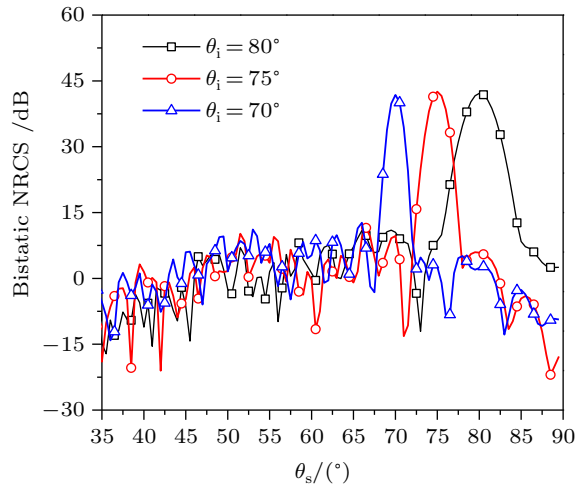


Fig. 9. (color online) Bistatic scattering of the model with different incident angles.

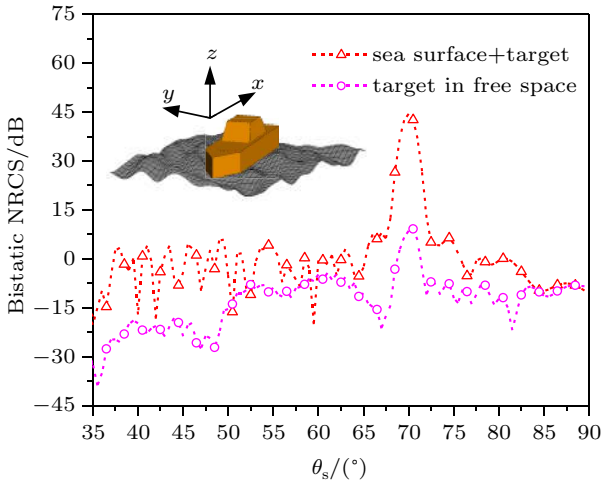


Fig. 10. (color online) Bistatic scattering from a ship-like target above Gaussian sea surface.

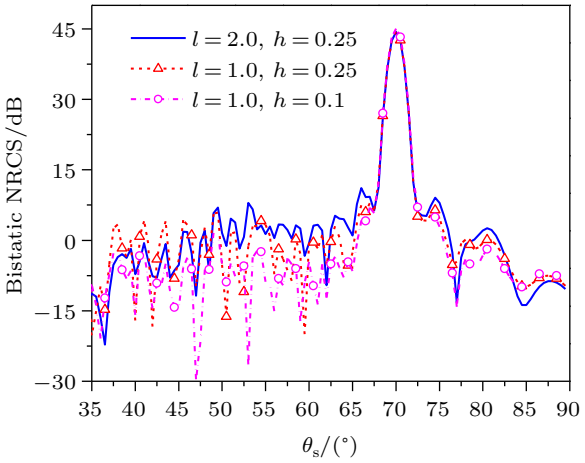


Fig. 11. (color online) Bistatic scattering of a ship-like target on the sea surface with different correlation lengths and RMS heights.

Figure 11 shows the results for different correlation lengths and RMS heights of the Gaussian rough surface. In contrast to the one discussed earlier in which the target is above the sea surface, in this example, the value in the mirror direction varies little when changing the sea surface roughness, and the difference in curves is mainly reflected in the direction away from the mirror. As discussed in the two examples, the PE-based method is feasible for solving bistatic scattering from 3-D targets and underlying rough surface at low grazing angle incidence regardless of whether the targets are on the sea surface or above it. In addition, numerical results of the coupling model under different incident angles are given in Fig. 12

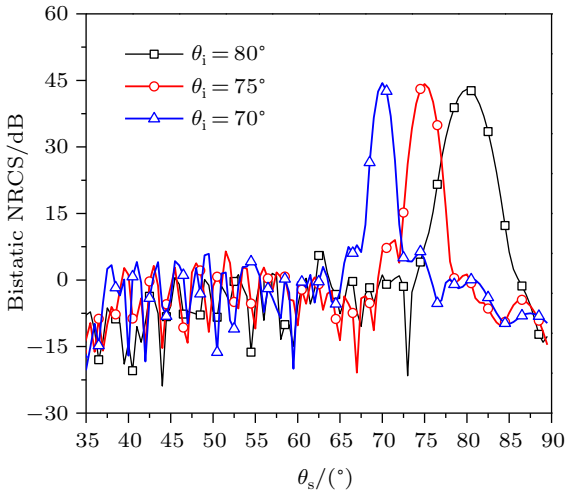


Fig. 12. (color online) Bistatic scattering of the model with different incident angles.

5. Conclusion

In this paper, an ADI high-order PE based method for solving composite electromagnetic scattering from 3-D electrically large targets and underlying randomly rough surface is presented. Some numerical examples under the tapered wave incidence at low grazing angles are given and discussed. The algorithm has been shown to provide accurate results and maintain high computational efficiency for solving the rough surfaces bistatic scattering problems. In addition, the PE-based method is not only suitable for the targets located above the rough surfaces, but also for the targets on the rough surfaces, as discussed in the examples. As a result of the preliminary study, the numerical tests show the feasibility of the proposed method, and the scattering problems in more complex computing scenarios will be further discussed. In addition, we are going to develop the algorithm via parallel processing technology to reduce the calculation load for the monostatic scattering problems and further improve the accuracy with the bidirectional algorithm.

References

[1] Guo L X, Gou X Y and Zhang L B 2014 *Chin. Phys. B* **23** 114102

[2] Pino M R, Landesa L, Rodriguez J L, Obelleiro and Burkholder R J 1999 *IEEE Trans. Antennas Propagat.* **47** 961

[3] Wang A Q, Guo L X and Chai C 2011 *Chin. Phys. B* **20** 050201

[4] Liu P and Jin Y Q 2004 *IEEE Trans. Antennas Propagat.* **52** 1205

[5] Jia C G, Guo L X and Yang P J 2015 *IEEE Antennas Wireless Propagat. Lett.* **14** 217

[6] Li J, Guo L X, Zeng H and Han X B 2009 *Chin. Phys. B* **18** 2757

[7] Ye H X and Jin Y Q 2007 *IEEE Trans. Geosci. Remote Sensing* **45** 1174

[8] Guo L X and Xu R W 2015 *IEEE Trans. Geosci. Remote Sensing* **53** 3885

[9] Leontovich M and Fock V 1946 *Acad. Sci. USSR. J. Phys.* **10** 13

[10] Levy M F and Zaporzhets A A 1998 *J. Acoust. Soc. Am.* **103** 735

[11] Zaporozhet A A and Levy 1999 *IEEE Trans. Antennas Propagat.* **47** 1688

[12] Levy M F 2000 *Parabolic Equation Methods For Electromagnetic Wave Propagation* (1st Edn.) (London: IEE Press) pp. 10–12

[13] Mallahzadeh A R, Soleimani M and Rashed-Mohassel J 2006 *Progress in Electromagnetics Research, PIER* **57** 265

[14] He Z, Fan Z H, Ding D Z and Chen R S 2015 *ACES Journal* **30** 496

[15] He Z and Chen R S 2015 *IEEE Trans. Antennas Propagat.* **63** 2595

[16] He Z and Chen R S 2016 *IEEE Trans. Antennas Propagat.* **64** 4777

[17] Pierson W J and Moskowitz L 1964 *J. Geophys. Res.* **69** 5181

[18] Martelly R and Janaswamy R 2009 *IEEE Trans. Antennas Propagat.* **57** 1759

[19] Collins M D 1993 *J. Acoust. Soc. Am.* **93** 1736

[20] Collins M D and Evans R B 1992 *J. Acoust. Soc. Am.* **91** 1357

[21] Ye H X and Jin Y Q 2005 *IEEE Trans. Antennas Propagat.* **53** 1234